

TURBULENCE IN A SELF-GRAVITATING MOLECULAR CLOUD CORE

SIYAO XU^{1,2} AND ALEX LAZARIAN¹

Draft version February 18, 2022

ABSTRACT

Externally driven interstellar turbulence plays an important role in shaping the density structure in molecular clouds. Here we study the dynamical role of internally driven turbulence in a self-gravitating molecular cloud core. Depending on the initial conditions and evolutionary stages, we find that a self-gravitating core in the presence of gravity-driven turbulence can undergo constant, decelerated, and accelerated infall, and thus has various radial velocity profiles. In the gravity-dominated central region, a higher level of turbulence results in a lower infall velocity, a higher density, and a lower mass accretion rate. As an important implication of this study, efficient reconnection diffusion of magnetic fields against the gravitational drag naturally occurs due to the gravity-driven turbulence, without invoking externally driven turbulence.

Subject headings: turbulence - magnetic fields - stars: formation

1. INTRODUCTION

The interstellar medium (ISM) is turbulent (e.g., Armstrong et al. (1995); Chepurnov & Lazarian (2010)). The interstellar turbulence plays a significant role in physical processes including the star formation (McKee & Ostriker 2007; Federrath & Klessen 2012), cosmic ray propagation (Scalo & Elmegreen 2004; Xu & Yan 2013; Xu et al. 2016; Xu & Lazarian 2018), dynamo amplification (Beck et al. 1996; Brandenburg & Subramanian 2005; Xu & Lazarian 2016, 2017b,a; Xu et al. 2019a) and turbulent reconnection (Lazarian & Vishniac 1999; Lazarian 2014; Lazarian et al. 2012) of interstellar magnetic fields, and formation and evolution of interstellar density structure (Padoan et al. 2001; Burkhardt et al. 2009; Xu et al. 2019b), accounting for observations, e.g., interstellar scattering of Galactic pulsars (Cordes et al. 1985; Rickett 1990; Xu & Zhang 2017), rotation measure fluctuations (Minter & Spangler 1996; Haverkorn et al. 2008; Xu & Zhang 2016), fluctuations in synchrotron intensity and polarization (Gaensler et al. 2011; Lazarian & Pogosyan 2012, 2016).

Supernova explosions are believed as a dominant source of turbulent energy on length scales of the order of 10 – 100 pc (Korpi et al. 1999; Haverkorn et al. 2008). The injected turbulence cascades down toward smaller length scales (Armstrong et al. 1995; Chepurnov & Lazarian 2010; Chepurnov et al. 2010; Qian et al. 2018). On small length scales in contracting dense cores in molecular clouds, an “adiabatic heating” mechanism acts to amplify the internal turbulence due to compression (Robertson & Goldreich 2012), where the gravitational potential energy is converted to the turbulent kinetic energy (Scalo & Pumphrey 1982; Sur et al. 2010). The resulting additional internal turbulent pressure support is expected to affect the dynamics and evolution of collapsing cores, as well as their density and velocity profiles (Lee et al. 2015; Murray & Chang 2015). In this study, we incorporate the gravity-driven turbulence and investigate the dynamical evolution of a spherical self-gravitating core. The self-similar behavior of a collapsing sphere has been extensively studied both analytically and numeri-

cally (Larson 1969; Penston 1969; Shu 1977; Hunter 1977; Foster & Chevalier 1993; Fatuzzo et al. 2004; Lou & Shen 2004). Here we follow the analytical approach of Shu (1977) to solve the hydrodynamic equations, but focus on the differences in solutions due to the presence of turbulence, which was not considered in the original formalism.

Apart from its importance in influencing the dynamics of molecular cloud cores, turbulence can also effectively enhance the diffusion efficiency of magnetic fields by enhancing their reconnection efficiency. In this work, we will also discuss the implication of gravity-driven turbulence on reconnection diffusion (RD) of magnetic fields. The paper is organized as follows. In §2, by solving the hydrodynamic equations involving the internal turbulent pressure, we analyze the dynamical effect of gravity-driven turbulence on the gravitational collapse of a spherical core. In §3, we discuss the implication on the RD of magnetic fields arising from the gravity-driven turbulence. The conclusions are provided in §4.

2. SELF-SIMILAR COLLAPSE OF A SELF-GRAVITATING TURBULENT SPHERE

We consider a spherical geometry for a self-gravitating and isothermal sphere. The governing equations include the continuity equation in terms of mass M , the continuity equation in terms of density ρ , and the momentum equation (Shu 1992):

$$\frac{\partial M}{\partial t} + u \frac{\partial M}{\partial r} = 0, \quad \frac{\partial M}{\partial r} = 4\pi r^2 \rho, \quad (1a)$$

$$\frac{\partial \rho}{\partial t} + \frac{1}{r^2} \frac{\partial (r^2 \rho u)}{\partial r} = 0, \quad (1b)$$

$$\frac{\partial u}{\partial t} + u \frac{\partial u}{\partial r} + \frac{1}{\rho} \frac{\partial (\rho v_t^2 + \rho a^2)}{\partial r} + \frac{GM}{r^2} = 0, \quad (1c)$$

where $|u|$ is the fluid speed, a is the sound speed, and v_t is the turbulent speed. In the absence of external driving, the turbulence in a contracting gas is amplified via the “adiabatic heating” mechanism, that is, turbulence adiabatically heats during contraction (Robertson & Goldreich 2012). On the other hand, the turbulence dissipates as the turbulent energy cascades toward smaller scales. Under the effects of “adiabatic heating” and dissipation of turbulence, v_t follows

¹ Department of Astronomy, University of Wisconsin, 475 North Charter Street, Madison, WI 53706, USA; sxu93@wisc.edu, lazarian@astro.wisc.edu

² Hubble Fellow

(Robertson & Goldreich 2012; Murray & Chang 2015):

$$\frac{\partial v_t}{\partial t} + u \frac{\partial v_t}{\partial r} + (1 + \eta \frac{v_t}{u}) \frac{v_t u}{r} = 0, \quad (2)$$

where the two terms in the brackets correspond to the turbulence driving and dissipation, respectively, and the parameter η represents the efficiency of turbulent energy cascade. Both the turbulent motion driven by gravitational contraction and the thermal motion of gas contribute to the pressure support against gravity in Eq. (1c).

To solve Eq. (1), we follow the analytical approach presented in Shu (1977) and combine the radius r and the time t into a dimensionless variable

$$x = \frac{r}{at}. \quad (3)$$

We then look for a similarity solution of the form

$$\begin{aligned} \rho(r, t) &= \frac{\alpha(x)}{4\pi G t^2}, & M(r, t) &= \frac{a^3 t}{G} m(x), \\ u(r, t) &= av(x), & v_t(r, t) &= C av(x), \end{aligned} \quad (4)$$

where the dimensionless variables α , m , and v are the reduced density, mass, and fluid speed, and G is the gravitational constant. Besides, $|C| \leq 1$ is the ratio of v_t to $|u|$ and also the ratio of the turbulent eddy-turnover rate to the gravitational contraction rate,

$$|C| = \frac{v_t/r}{|u|/r}. \quad (5)$$

For the contraction induced turbulence, both simulations and physical considerations suggest that v_t tracks $|u|$ and tends to synchronize with $|u|$ (Robertson & Goldreich 2012; Murray & Chang 2015).³ Therefore, we consider C as a constant.

By substituting Eq. (4) into Eqs. (1) and (2), we find

$$m = x^2 \alpha (x - v), \quad (6a)$$

$$\begin{aligned} &\left\{ (x - v)[(x - v) - 2C^2 v] - (1 + C^2 v^2) \right\} \frac{dv}{dx} \\ &= (x - v) \left[\alpha(x - v) - \frac{2}{x}(1 + C^2 v^2) \right], \end{aligned} \quad (6b)$$

$$\begin{aligned} &\left\{ (x - v)[(x - v) - 2C^2 v] - (1 + C^2 v^2) \right\} \frac{d\alpha}{dx} \\ &= \alpha(x - v) \left\{ \alpha - \frac{2}{x}[(x - v) - 2C^2 v] \right\}, \end{aligned} \quad (6c)$$

$$(x - v) \frac{dv}{dx} = (1 + \eta C) \frac{v^2}{x}. \quad (6d)$$

The ratio of the gravitational force to the pressure gradient force is

$$\mathcal{R} = \frac{\frac{GM}{r^2}}{\frac{1}{\rho} \frac{\partial(\rho v_t^2 + \rho a^2)}{\partial r}} \sim \frac{\alpha x(x - v)}{C^2 v^2 + 1}, \quad (7)$$

where the expressions in Eqs. (4) and (6a) are used. If the effect of turbulence is negligible, it becomes

$$\mathcal{R}_{\text{the}} \sim \alpha x(x - v). \quad (8)$$

For the ‘‘inside-out’’ collapse of a singular isothermal sphere considered in Shu (1977), the hydrodynamic signal propagates at the speed of sound. The envelope at $x > 1$ can remain

³ The synchronization is expected to be stable as the turbulent eddies are compressed on their turnover timescales (Robertson & Goldreich 2012).

in the initial hydrostatic state, while the interior at $x < 1$ undergoes gravitational infall. Here we incorporate the effect of self-driven turbulence. In the case of highly supersonic turbulence, i.e., $Cv \gg 1$, \mathcal{R} is approximately

$$\mathcal{R}_{\text{tur}} \sim \frac{\alpha x(x - v)}{C^2 v^2}, \quad (9)$$

which is smaller than \mathcal{R}_{the} .

In various asymptotic limits, the solution to the coupled Eqs. (6b) and (6c) has different behaviors. We start with the limit $x \gg |v|$, i.e., $r \gg |u|t \geq v_t t$. It is beyond the radius where the hydrodynamic signals carried by turbulence can reach. We consider different cases with small and large initial infall velocities.

Case (1): $x \rightarrow \infty$ ($t \rightarrow 0$), $v \rightarrow 0$, $\alpha \ll 1$.

At an initial state, if the infall velocity is sufficiently small, the effect of turbulence is negligible. This initial state can be treated as the case of collapse of a singular isothermal sphere at a large x considered in Shu (1977), where turbulence was not taken into account. One can easily obtain the solution:

$$v = -(A - 2)x^{-1}, \quad (10a)$$

$$\alpha = Ax^{-2}, \quad (10b)$$

and

$$m \approx \alpha x^3 = Ax, \quad (11)$$

where the constant A should not be smaller than 2 as $v(\leq 0)$ is an inward velocity.

Case (2): $x \rightarrow \infty$ ($t \rightarrow 0$), $Cv \gg 1$, $\alpha \ll 1$.

This initial condition with a large infall velocity allows the generation of supersonic turbulence. Accordingly, Eqs. (6b) and (6c) can be approximated by:

$$\frac{dv}{dx} = \alpha - \frac{2C^2 v^2}{x^2}, \quad (12a)$$

$$x \frac{d\alpha}{dx} = -2\alpha, \quad (12b)$$

We find the solution

$$v \approx -v_2, \quad (13a)$$

$$\alpha = \alpha_2 x^{-2}, \quad (13b)$$

where v_2 and α_2 are constants and $\alpha_2 \leq 2C^2 v_2^2$. With the same density profile as in Case (1), the asymptotic form of m is the same as Eq. (11),

$$m \approx \alpha_2 x. \quad (14)$$

To have a constant v , it requires $\eta = -1/C$ (Eq. (6d)). With comparable rates of turbulence driving and dissipation, the resulting turbulence has a constant v_t . The above result shows that the system has undisturbed infall motions.

The different initial conditions in Case (1) and Case (2) lead to different behaviors of the subsequent collapse. We next consider the limit $x \ll |v|$, i.e., $r \ll |u|t$, and rewrite Eqs. (6b) and (6c) as

$$\frac{dv}{dx} = \frac{1}{1 + C^2} \left(\alpha + \frac{2C^2}{x} v \right), \quad (15a)$$

$$\frac{d\alpha}{dx} = -\frac{\alpha}{(1 + C^2)v} \left[\alpha + \frac{2(1 + 2C^2)}{x} v \right]. \quad (15b)$$

The ratio of the two terms in the brackets in Eq. (15a) reflects the relative importance of gravitational contraction and turbulent pressure support (see Eq. (9)). In the regime where the turbulent pressure plays a dominant role, i.e., $\mathcal{R}_{\text{tur}} \ll 1$, we can further simplify the above equations and have

$$\frac{dv}{dx} = \frac{2C^2}{1+C^2} \frac{v}{x}, \quad (16a)$$

$$\frac{d\alpha}{dx} = -\frac{2(1+2C^2)}{1+C^2} \frac{\alpha}{x}, \quad (16b)$$

We derive the solutions as

$$v = -v_1 x^{\frac{2C^2}{1+C^2}}, \quad (17a)$$

$$\alpha = \alpha_1 x^{-\frac{2(1+2C^2)}{1+C^2}}, \quad (17b)$$

where v_1 and α_1 are constants. As $|v|$ decreases with decreasing x , it shows that the turbulent pressure dominates the dynamics and causes deceleration of the infall. Given the above expressions, m (Eq. (6a)) is approximately

$$m \approx \alpha_1 v_1. \quad (18)$$

By comparing Eq. (16a) with Eq. (6d), we find that the corresponding relation between η and C is

$$\eta = -\frac{1+3C^2}{C(1+C^2)}. \quad (19)$$

With $\eta|C| > 1$, the dissipation is more efficient than driving. Thus v_t decreases with decreasing x .

In the regime where the gravitational contraction is more important than the turbulent support, i.e., $\mathcal{R}_{\text{tur}} \geq 1$, the solution to Eq. (15) is

$$v = -\frac{2\alpha_0}{1+5C^2} x^{-\frac{1}{2}}, \quad (20a)$$

$$\alpha = \alpha_0 x^{-\frac{3}{2}}, \quad (20b)$$

and

$$m \approx \frac{2\alpha_0^2}{1+5C^2}, \quad (21)$$

where α_0 is a constant. The above result has the same scaling as that of a free-fall collapse, as expected in the regime dominated by self-gravity. Eq. (20a) indicates the relation

$$\eta \sim -\frac{1}{2C}, \quad (22)$$

showing enhanced turbulence toward smaller x with $\eta|C| < 1$. The above relations between C and η in both regimes with decelerated and accelerated infall, i.e., Eq. (19) with $C = -1$ and Eq. (22), are consistent with earlier numerical simulations of contracting turbulence (Robertson & Goldreich 2012).

In Case (1) with an initially small infall velocity, the numerical solution to Eqs. (6b) and (6c) in the entire range of x is presented in Fig. 1. Our analytical scalings well describe its asymptotic behaviors. From the envelope to the inner region, \mathcal{R} changes from (Eqs. (8) and (10b))

$$\mathcal{R}_{\text{the}} \sim \alpha x^2 = A \quad (23)$$

to (Eqs. (9) and (20))

$$\mathcal{R}_{\text{tur}} \sim -\frac{\alpha x}{C^2 v} = \frac{1+5C^2}{2C^2}. \quad (24)$$

Due to the turbulent support, \mathcal{R} remains constant, which would otherwise increase as $x \rightarrow 0$ in a free-fall regime (Shu 1977). Comparing the cases with different values of C , we see that turbulence in the inner region results in a lower infall velocity, a higher ρ , and a lower constant rate of mass accretion onto a central mass point

$$\dot{M} = \frac{\partial M(0, t)}{\partial t} = \frac{a^3 m(0)}{G} \quad (25)$$

compared to the free-fall case.

In contrast, in Case (2) with an initially large infall velocity, the numerical result in the entire range of x is displayed in Fig. 2. We see three different regimes with (i) constant infall, (ii) decelerated infall, and (iii) accelerated infall. To better illustrate the asymptotic scalings in the dynamically unstable regimes (ii) and (iii), Fig. 3 presents the solutions for $x < |v|$ with the boundary condition given by Eq. (17). From regime (ii) to regime (iii), \mathcal{R} changes from (Eqs. (9) and (17))

$$\mathcal{R}_{\text{tur}} \sim -\frac{\alpha x}{C^2 v} = \frac{\alpha_1}{C^2 v_1} x^{-\frac{1+5C^2}{1+C^2}}, \quad (26)$$

which increases with decreasing x , to \mathcal{R}_{tur} expressed in Eq. (24). The change of \mathcal{R}_{tur} clearly indicates the transition from turbulent pressure- to gravity-dominated dynamics. Besides, from Figs. 2(c) and 3(c), we find that the change of m in regimes (ii) and (iii) is insignificant and it approaches constant toward a small x , leading to a flat radial profile of M and a constant \dot{M} as in Case (1).

The above results clearly demonstrate the importance of gravity-driven turbulence in affecting the collapse dynamics. Compared with the isothermal collapse with only thermal pressure, turbulence provides additional pressure support against the self-gravity and enables deceleration of the infall. Compared with the adiabatic collapse where the released gravitational energy is absorbed, due to the dissipation of turbulent energy, the gravity-driven turbulence is incapable of halting the gravitational contraction. At a sufficiently small x , the solution has the free-fall scaling. Fig. 4 shows the numerically solved $-u(r, t)$, the number density of atomic hydrogen $n_H(r, t) = \rho(r, t)/m_H$, where m_H is the mass of hydrogen atom, and $M(r, t)$. As a comparison, we present both cases of a non-turbulent collapse with a quasi-static envelope (Figs. 4(a), 4(c), and 4(e), corresponding to Fig. 1(a) with $C = 0$) and a turbulent collapse with an initially large infall velocity (Figs. 4(b), 4(d), and 4(f), corresponding to Figs. 2(a) and 2(b) with $C = -1$). Note that we adopt the values of parameters here only for illustrative purposes, but not for detailed comparisons with specific observations. In the former case, we can easily see that the outward moving expansion wavefront separates the free-fall regime and the quasi-static regime. While in the latter case the collapse exhibits a more complex behavior. Comparing the two scenarios, despite the different initial conditions and different levels of turbulence, the same scalings of velocity, density, and mass apply to the central region after a sufficiently long time, showing the dominance of self-gravity at the center.

3. DISCUSSION

In the presence of turbulence, the stochastic wandering of magnetic field lines naturally takes place as a result of turbulent energy cascade and turbulent mixing of magnetic fields. Consequently, the reconnection of wandering magnetic fields

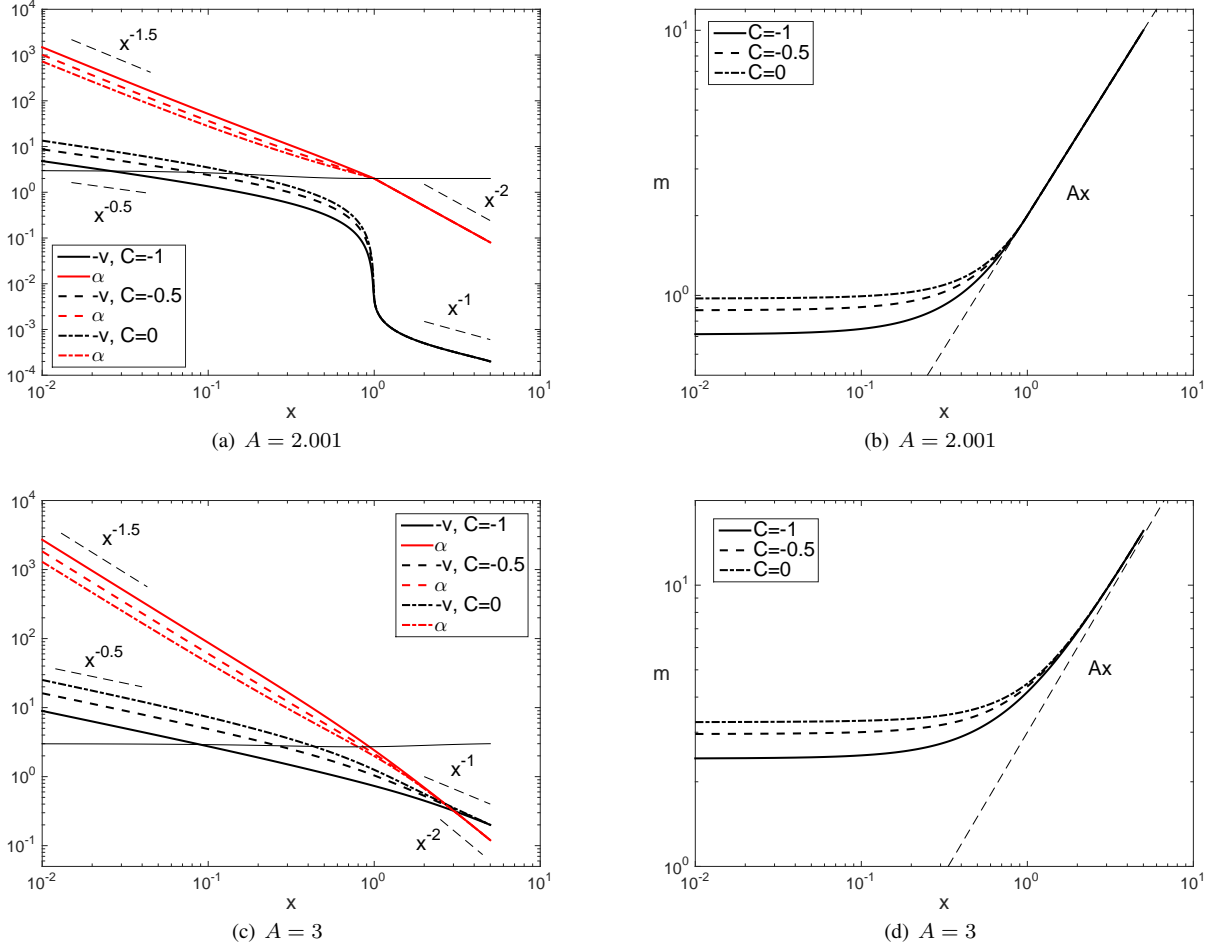


FIG. 1.— Similarity solutions for $-v$, α ((a) and (c)), and m ((b) and (d)) in Case (1) with the initial condition given by Eq. (10). The thin solid line in (a) and (c) indicates \mathcal{R} (Eq. (7)) with $C = -1$. The short dashed lines indicate the analytically derived asymptotic scalings.

are much more efficient than the microscopic magnetic reconnection (Lazarian & Vishniac 1999). The latter relies on the resistive diffusion in a conducting fluid or the ambipolar diffusion in a partially ionized medium. On length scales where turbulence exists, it is the turbulent diffusion of magnetic fields that dominates over the above microscopic diffusion processes. The turbulent reconnection of magnetic fields violates flux freezing and allows turbulent diffusion of magnetic fields, which has been termed “reconnection diffusion (RD)” (Lazarian 2005). The diffusion rate only depends on the turbulence properties (Kowal et al. 2009).

To illustrate the effect of RD induced by gravity-driven turbulence, in Fig. 5, we present the evolution of magnetic field profile in the decelerated infall regime in Case (2) (see Appendix A for the detailed calculations). We see that the RD rapidly balances the gravitational drag and stabilizes the magnetic field profile to have the form consistent with Eq. (A4),

$$B_s(r) = 10 \mu\text{G} \left(\frac{r}{0.1 \text{ pc}} \right)^{-1}. \quad (27)$$

It suggests that the RD results in an efficient expulsion of magnetic fields and prevents the accumulation of magnetic flux in a collapsing region.

The application of RD to star formation processes (Santos-Lima et al. 2010; Lazarian et al. 2012; Leão et al.

2013; Lazarian 2014; Li et al. 2015; Mocz et al. 2017) demonstrates that RD leads to violation of flux-freezing (Eyink et al. 2013) and is indispensable for solving the “magnetic flux problem” (Mestel & Spitzer 1956), accounting for the observed supercritical molecular clouds and cores (Crutcher et al. 2010) and the observed strengths of surface magnetic fields of stars (Johns-Krull et al. 2004). RD also mitigates the magnetic braking “catastrophe” and allows the formation of centrifugally supported circumstellar disks (Santos-Lima et al. (2012, 2013); González-Casanova et al. (2016); see also Gray et al. (2018)). Most earlier studies on RD involved externally driven turbulence, e.g., the interstellar turbulence driven by supernova explosions on large scales.⁴ Differently, here we find that RD naturally occurs during the gravitational collapse without an external source for driving turbulence.

In a weakly ionized and magnetized core, besides RD, the ambipolar diffusion (AD) of magnetic fields due to ion-neutral drift also takes place. The comparison between the

⁴ In most MHD simulations of the interstellar turbulence, turbulence is continuously forced at a large driving scale to simulate the externally driven turbulence for a system on scales smaller than the driving scale of turbulence. In the simulations with decaying turbulence, additional turbulence can be internally driven after the gravitational contraction of the system initiates.

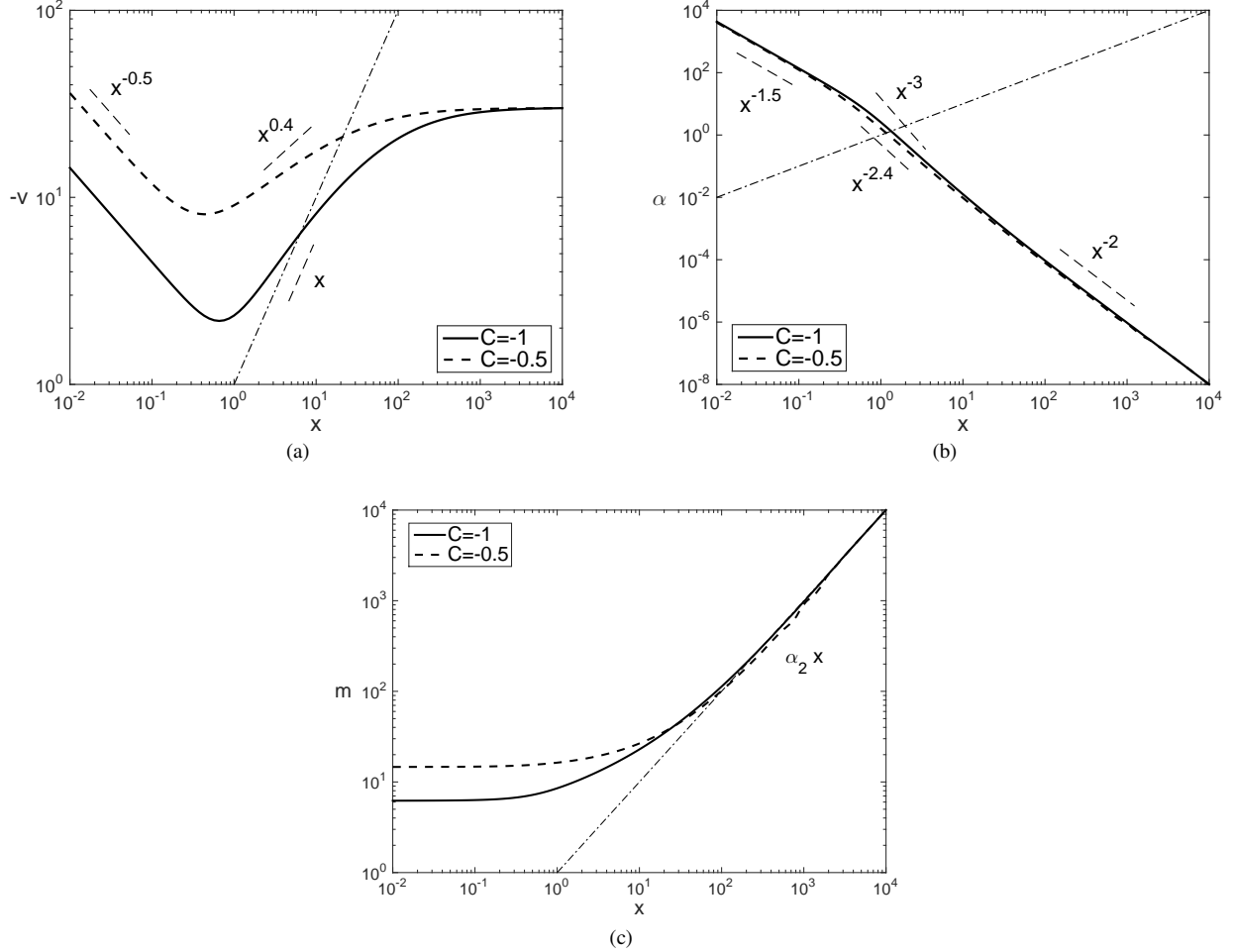


FIG. 2.— Similarity solutions in Case (2) with the initial condition given by Eq. (13), where $v_2 = 30$ and $a_2 = 1$. The dash-dotted line denotes $|v| = x$ in (a) and (b).

rates of AD and RD shows

$$\begin{aligned} \frac{\omega_d}{v_t/r} &= \frac{\xi_n V_A^2}{6\nu_{ni} v_t r} = \frac{\xi_n v_t}{6\nu_{ni} r} \\ &= 3.2 \times 10^{-4} \left(\frac{v_t}{0.1 \text{ km s}^{-1}} \right) \left(\frac{r}{0.1 \text{ pc}} \right)^{-1} \\ &\quad \left(\frac{n_H}{10^4 \text{ cm}^{-3}} \right)^{-1} \left(\frac{n_e/n_H}{10^{-6}} \right)^{-1}, \end{aligned} \quad (28)$$

where $\xi_n = \rho_n/\rho$ is the neutral fraction with the neutral mass density ρ_n and the total mass density ρ , $\nu_{ni} = \gamma_d \rho_i$ is the neutral-ion collision frequency with the drag coefficient $\gamma_d = 3.5 \times 10^{13} \text{ cm}^3 \text{ g}^{-1} \text{ s}^{-1}$ (Draine et al. 1983; Shu 1992) and the ion mass density ρ_i , and n_H and n_e are number densities of the atomic hydrogen and electrons. Here we also assume $v_t = V_A$, where V_A is the Alfvén speed, and $m_i = 29m_H$, $m_n = 2.3m_H$ as the mean molecular mass of ions and neutrals in a core (Shu 1992), where m_H is the hydrogen atomic mass. Evidently, in the presence of turbulence, AD is subdominant compared to RD.

4. CONCLUSIONS

The effect of turbulence on gas dynamics varies with the length scale of interest. For the interstellar turbulence with a driving scale $\sim 50 - 100$ pc, shear Alfvénic

motions and compressive motions in supersonic turbulence play an important role in shaping the density structures within the inertial range of the interstellar turbulence (Padoan et al. 2001; Federrath et al. 2010; Xu & Zhang 2016, 2017; Robertson & Goldreich 2018; Mocz & Burkhardt 2018). For the gravity-driven turbulence in a contracting core considered here, the driving scale is small, and thus the internal turbulent motions provide pressure support for the surrounding density shells. We found that the gravity-driven turbulence can slow down the gravitational infall and mass accretion.

Compared with the Kolmogorov scaling $v_t \propto r^{1/3}$ (e.g., Qian et al. (2018)) or the Larson’s scaling $v_t \propto r^{1/2}$ (Larson 1981; Myers 1983) in the inertial range of externally driven turbulence, we found that the gravity-driven turbulence can give rise to various velocity dispersion profiles, $v_t \propto r^\alpha$ with $0 \leq \alpha \leq 1$ in the outer region of a dynamically contracting core at an early time of its evolution, and $v_t \propto r^{-1/2}$ toward the center in a quasi-statically contracting core or a dynamically contracting core at a late time of its evolution (Fig. 4). Our analytical scalings are consistent with earlier numerical results in the parameter space of the simulations (Robertson & Goldreich 2012). Observations suggest that the non-thermal line width-size relation of massive cores is flatter than that of low-mass cores (Caselli & Myers 1995). Plume et al. (1997) found no statistically significant

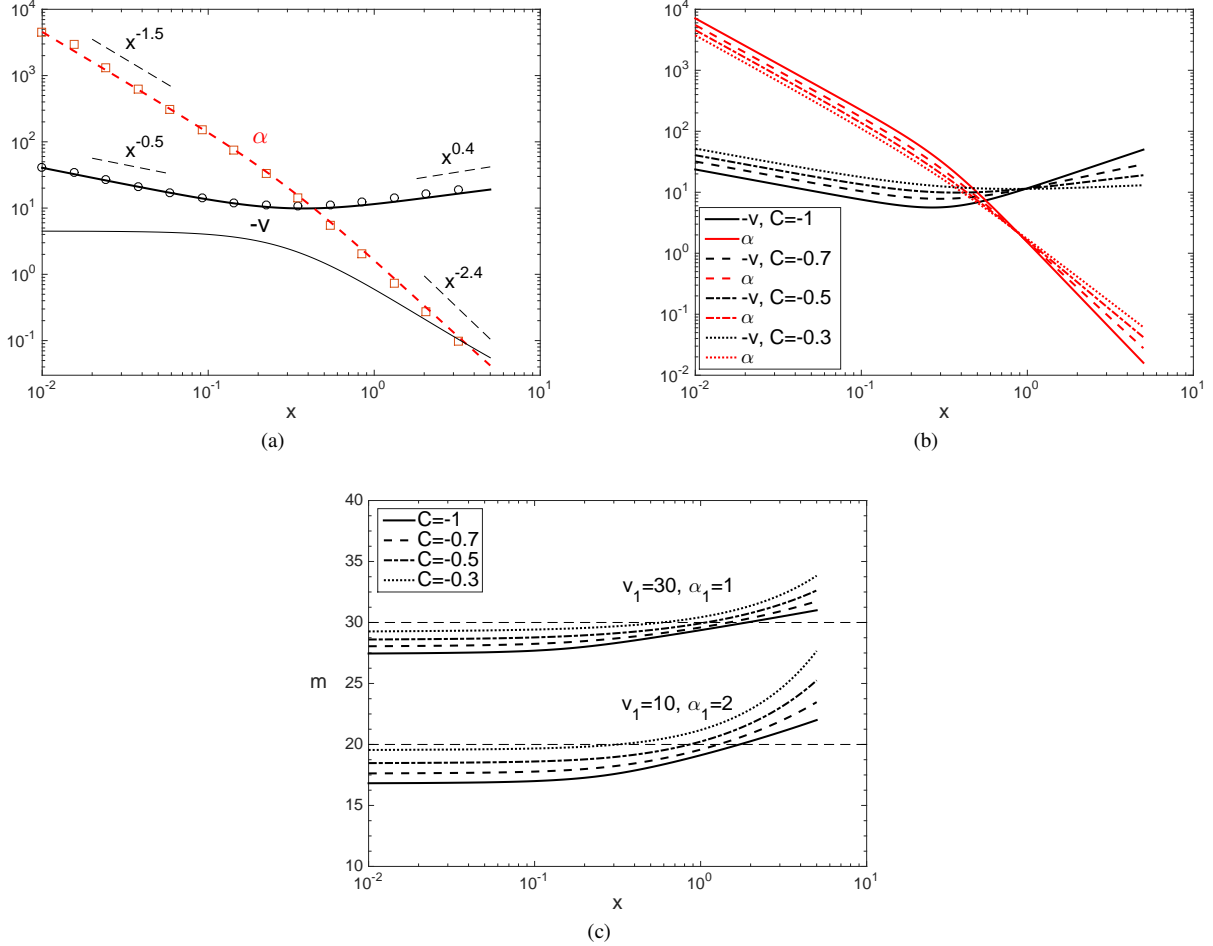


FIG. 3.— Similarity solutions with the boundary condition given by Eq. (17). $v_1 = 10$ and $\alpha_1 = 2$ are adopted for (a) and (b). In (a), $C = -0.5$, and the thin solid line indicates \mathcal{R} at $C = -0.5$. Circles represent the solution derived with the boundary condition given by Eq. (20) at a small x . The thin dashed lines in (c) denote the asymptotic value of m given by Eq. (18).

line width-size relationship or a positive correlation between line width and density for very massive cores. These unexpected observational findings support the theoretical picture of gravity-driven turbulence in molecular cloud cores (see also Murray & Chang (2015)). More detailed and quantitative comparisons will be carried out in our future work.

As an important implication of the current study, the gravity-driven turbulence not only influences the dynamics of a collapsing core, but also enables an efficient diffusion of magnetic fields. At the balance between the gravitational drag and diffusion, a stationary radial profile of magnetic field can be reached, with the slope depending on the fraction

of gravitational potential energy converted to the turbulent kinetic energy.

S.X. acknowledges the support for Program number HST-HF2-51400.001-A provided by NASA through a grant from the Space Telescope Science Institute, which is operated by the Association of Universities for Research in Astronomy, Incorporated, under NASA contract NAS5-26555. A.L. acknowledges the support from grant NSF DMS 1622353.

APPENDIX

RD DUE TO GRAVITY-DRIVEN TURBULENCE

Here we consider gravitational contraction of weak magnetic fields as suggested by observations (Crutcher et al. 2010). Since the gravitational drag only occurs along the radial direction, we adopt the one-dimensional induction equation, i.e., the magnetic convection-diffusion equation (Luhmann et al. 1984),

$$\frac{\partial B}{\partial t} = -\frac{\partial}{\partial r}(Bu) + \frac{\partial}{\partial r}\left(\kappa \frac{\partial B}{\partial r}\right), \quad (\text{A1})$$

to discuss the RD of dynamically insignificant magnetic fields. The first term on the RHS of Eq. (A1) describes the magnetic fields being dragged inward with the infalling flow, which alone corresponds to flux freezing. The second term describes the RD of magnetic fields, where the diffusion coefficient is

$$\kappa = v_t r = C u r \quad (\text{A2})$$

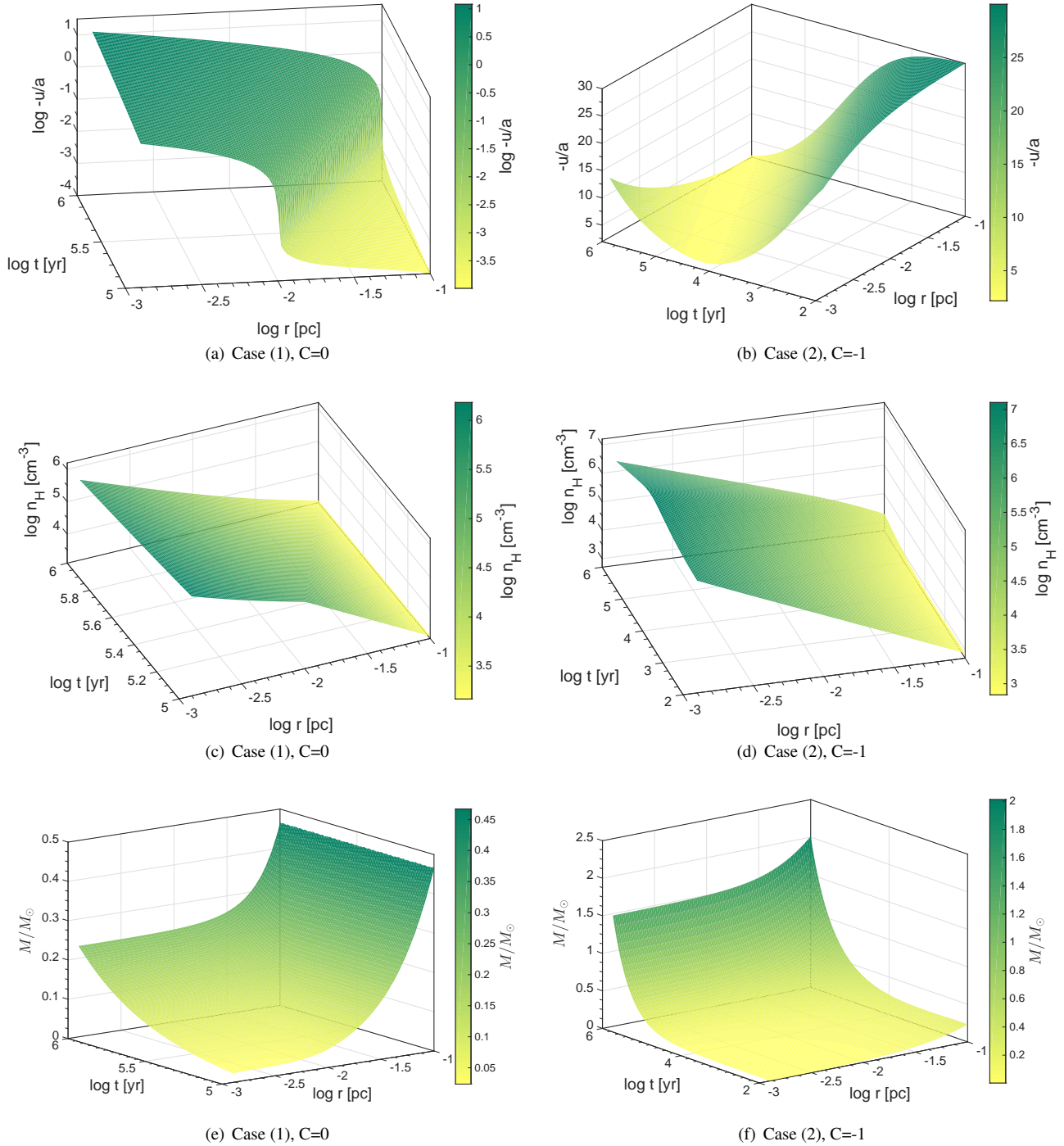


FIG. 4.— Time evolution of the radial profiles of $-u(r, t)$ (normalized by a), $n_H(r, t)$, and $M(r, t)$ (normalized by M_\odot) in Case (1) with $C = 0$ and $A = 2.001$ ((a), (c), and (e)) and in Case (2) with $C = -1$, $v_2 = 30$, and $\alpha_2 = 1$ ((b), (d), and (f)).

for super-Alfvénic turbulence with the turbulent energy exceeding the magnetic energy.

Under the effect of RD, when the diffusive term becomes comparable to the convective term, i.e.,

$$Bu = \kappa \frac{\partial B}{\partial r}, \quad (\text{A3})$$

the evolution of magnetic fields reaches a steady state. The steady-state magnetic field is

$$B_s(r) = B_f \left(\frac{r}{r_f} \right)^{\frac{1}{C}}, \quad (\text{A4})$$

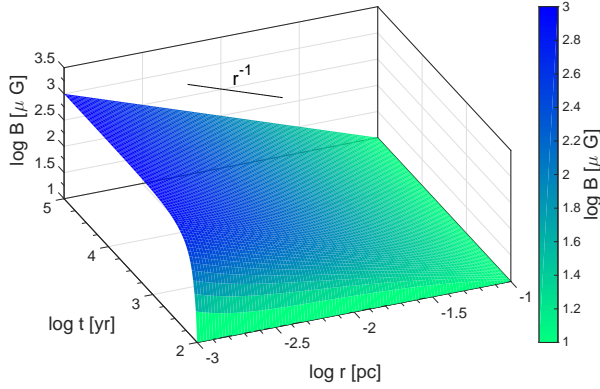


FIG. 5.— Time evolution of magnetic field profile as the numerical solution to Eq. (A1) in the decelerated infall regime in Case (2), with $v_1 = 10$ (Eq. (17a)) and $C = -1$. The initial uniform magnetic field has a strength $10 \mu\text{G}$.

where B_f is the field strength at a reference radius r_f . We see that $B_s(r)$ does not depend on the functional form of u as it is canceled out in Eq. (A3), but only depends on C .

REFERENCES

- Armstrong, J. W., Rickett, B. J., & Spangler, S. R. 1995, *ApJ*, 443, 209
 Beck, R., Brandenburg, A., Moss, D., Shukurov, A., & Sokoloff, D. 1996, *ARA&A*, 34, 155
 Brandenburg, A., & Subramanian, K. 2005, *Phys. Rep.*, 417, 1
 Burkhart, B., Falceta-Gonçalves, D., Kowal, G., & Lazarian, A. 2009, *ApJ*, 693, 250
 Caselli, P., & Myers, P. C. 1995, *ApJ*, 446, 665
 Chepurnov, A., & Lazarian, A. 2010, *ApJ*, 710, 853
 Chepurnov, A., Lazarian, A., Stanimirović, S., Heiles, C., & Peek, J. E. G. 2010, *ApJ*, 714, 1398
 Cordes, J. M., Weisberg, J. M., & Boriakoff, V. 1985, *ApJ*, 288, 221
 Crutcher, R. M., Wandelt, B., Heiles, C., Falgarone, E., & Troland, T. H. 2010, *ApJ*, 725, 466
 Draine, B. T., Roberge, W. G., & Dalgarno, A. 1983, *ApJ*, 264, 485
 Eyink, G., et al. 2013, *Nature*, 497, 466
 Fatuzzo, M., Adams, F. C., & Myers, P. C. 2004, *ApJ*, 615, 813
 Federrath, C., & Klessen, R. S. 2012, *ApJ*, 761, 156
 Federrath, C., Roman-Duval, J., Klessen, R. S., Schmidt, W., & Mac Low, M.-M. 2010, *A&A*, 512, A81
 Foster, P. N., & Chevalier, R. A. 1993, *ApJ*, 416, 303
 Gaensler, B. M., et al. 2011, *Nature*, 478, 214
 González-Casanova, D. F., Lazarian, A., & Santos-Lima, R. 2016, *ApJ*, 819, 96
 Gray, W. J., McKee, C. F., & Klein, R. I. 2018, *MNRAS*, 473, 2124
 Haverkorn, M., Brown, J. C., Gaensler, B. M., & McClure-Griffiths, N. M. 2008, *ApJ*, 680, 362
 Hunter, C. 1977, *ApJ*, 218, 834
 Johns-Krull, C. M., Valenti, J. A., & Saar, S. H. 2004, *ApJ*, 617, 1204
 Korpi, M., Brandenburg, A., Shukurov, A., & Tuominen, I. 1999, in *Interstellar Turbulence*, ed. J. Franco & A. Carraminana, 127
 Kowal, G., Lazarian, A., Vishniac, E. T., & Otmianowska-Mazur, K. 2009, *ApJ*, 700, 63
 Larson, R. B. 1969, *MNRAS*, 145, 271
 —. 1981, *MNRAS*, 194, 809
 Lazarian, A. 2005, in *American Institute of Physics Conference Series*, Vol. 784, *Magnetic Fields in the Universe: From Laboratory and Stars to Primordial Structures.*, ed. E. M. de Gouveia dal Pino, G. Lugones, & A. Lazarian, 42–53
 Lazarian, A. 2014, *Space Sci. Rev.*, 181, 1
 Lazarian, A., Esquivel, A., & Crutcher, R. 2012, *ApJ*, 757, 154
 Lazarian, A., & Pogosyan, D. 2012, *ApJ*, 747, 5
 —. 2016, *ApJ*, 818, 178
 Lazarian, A., & Vishniac, E. T. 1999, *ApJ*, 517, 700
 Leão, M. R. M., de Gouveia Dal Pino, E. M., Santos-Lima, R., & Lazarian, A. 2013, *ApJ*, 777, 46
 Lee, E. J., Chang, P., & Murray, N. 2015, *ApJ*, 800, 49
 Li, P. S., McKee, C. F., & Klein, R. I. 2015, *MNRAS*, 452, 2500
 Lou, Y.-Q., & Shen, Y. 2004, *MNRAS*, 348, 717
 Luhmann, J. G., Russell, C. T., & Elphic, R. C. 1984, *J. Geophys. Res.*, 89, 362
 McKee, C. F., & Ostriker, E. C. 2007, *ARA&A*, 45, 565
 Mestel, L., & Spitzer, Jr., L. 1956, *MNRAS*, 116, 503
 Minter, A. H., & Spangler, S. R. 1996, *ApJ*, 458, 194
 Mocz, P., & Burkhart, B. 2018, *MNRAS*, 480, 3916
 Mocz, P., Burkhart, B., Hernquist, L., McKee, C. F., & Springel, V. 2017, *ApJ*, 838, 40
 Murray, N., & Chang, P. 2015, *ApJ*, 804, 44
 Myers, P. C. 1983, *ApJ*, 270, 105
 Padoan, P., Juvela, M., Goodman, A. A., & Nordlund, Å. 2001, *ApJ*, 553, 227
 Penston, M. V. 1969, *MNRAS*, 144, 425
 Plume, R., Jaffe, D. T., Evans, II, N. J., Martín-Pintado, J., & Gómez-González, J. 1997, *ApJ*, 476, 730
 Qian, L., Li, D., Gao, Y., Xu, H., & Pan, Z. 2018, *ApJ*, 864, 116
 Rickett, B. J. 1990, *ARA&A*, 28, 561
 Robertson, B., & Goldreich, P. 2012, *ApJ*, 750, L31
 —. 2018, *ApJ*, 854, 88
 Santos-Lima, R., de Gouveia Dal Pino, E. M., & Lazarian, A. 2012, *ApJ*, 747, 21
 —. 2013, *MNRAS*, 429, 3371
 Santos-Lima, R., Lazarian, A., de Gouveia Dal Pino, E. M., & Cho, J. 2010, *ApJ*, 714, 442
 Scalo, J., & Elmegreen, B. G. 2004, *ARA&A*, 42, 275
 Scalo, J. M., & Pumphrey, W. A. 1982, *ApJ*, 258, L29
 Shu, F. H. 1977, *ApJ*, 214, 488
 —. 1992, *The physics of astrophysics. Volume II: Gas dynamics*.
 Sur, S., Schleicher, D. R. G., Banerjee, R., Federrath, C., & Klessen, R. S. 2010, *ApJ*, 721, L134
 Xu, S., Garain, S. K., Balsara, D. S., & Lazarian, A. 2019a, *ApJ*, 872, 62
 Xu, S., Ji, S., & Lazarian, A. 2019b, *ApJ*, 878, 157
 Xu, S., & Lazarian, A. 2016, *ApJ*, 833, 215
 —. 2017a, *ApJ*, 850, 126
 —. 2017b, *New Journal of Physics*, 19, 065005
 —. 2018, *ApJ*, 868, 36
 Xu, S., & Yan, H. 2013, *ApJ*, 779, 140
 Xu, S., Yan, H., & Lazarian, A. 2016, *ApJ*, 826, 166
 Xu, S., & Zhang, B. 2016, *ApJ*, 824, 113
 —. 2017, *ApJ*, 835, 2